ACS Catalysis

pubs.acs.org/acscatalysis
Research Article

Origin of Catalysis by the $[Ga_4L_6]^{12-}$ Metallocage on the Prins Reaction

Iker Zapirain-Gysling, Gantulga Norjmaa, Jean Didier Maréchal, and Gregori Ujaque*

Cite This: ACS Catal. 2024, 14, 18722−18733
Read Online

ACCESS | Metrics & More | Article Recommendations | Supporting Information

ABSTRACT: The Prins cyclization of citronellal is a significant reaction for synthesizing new carbon−carbon bonds, typically catalyzed by acidic conditions, serving as a crucial industrial intermediate for menthol production. The present work aims to investigate, by means of computational methods, the host−guest catalytic mechanism within the $[Ga_4L_6]^{12-}$ metallocage, which promotes the formation of minor alkene products, emulating the selectivity observed in biological terpene synthases. A combination of molecular dynamics simulations, DFT, and QM/MM calculations was employed to explore the reaction profiles, revealing the dynamics of encapsulation and the role of protonation and cyclization steps. Our study confirms that the metallocage does not directly modify the reaction but rather provides a unique microenvironment within its cavity that facilitates acid-catalyzed reactions under basic or neutral conditions in solution. Indeed, modification of the basicity of the citronellal reactant once encapsulated turns out to be critical for the process. Moreover, conversely to what is expected, the metallocage does not promote a conformational preorganization of the guest to a more compact conformation prone to undertake the cyclization. Identifying these factors offers a detailed understanding of rate enhancement by metallocages that can be of general applicability.

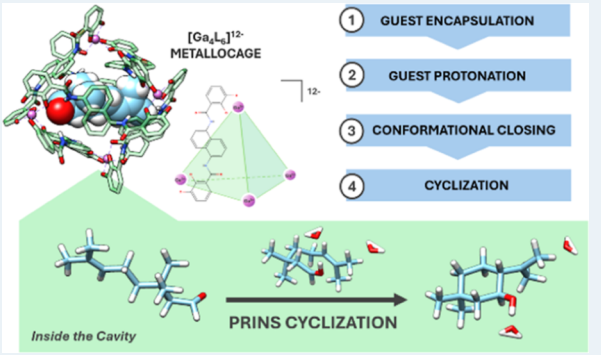

KEYWORDS: *Prins reaction, supramolecular chemistry, Metal−organic cages (MOCs), supramolecular catalysis, Host−guest interactions, computational chemistry, reaction mechanisms, molecular modeling*

INTRODUCTION

The development of synthetic hosts possessing a cavity with the ability of accelerating chemical reactions is one of the main goals of research in catalysis.[1] Among these supramolecular structures, metal−organic cages (MOCs) are among the most interesting ones.[2−6] These metallocages are formed with metals acting as connecting points and organic ligands as edges or faces, creating space-constrained cavities; this type of supramolecular system opens a myriad of possibilities of molecular shapes and sizes.[7−11] Indeed, MOCs have proven to be able to accelerate reaction rates compared to their analogous bulk solution reactions for many processes.[12−19]

One of the reactions where application of MOCs has been developed is in the synthesis of terpenoids. Terpene synthases are essential in nature by catalyzing the biosynthesis of terpenoids, a broad family of natural compounds. With over 76,000 characterized members, terpenoids exhibit remarkable structural intricacy, gaining significant attention in the industry due to their diverse applications, ranging from flavors and fragrances to pharmaceuticals and biofuels.[20−22] In this context, exploring the catalytic synthesis of terpenoids offers promising paths for the development of greener and more efficient processes.

Over the last years, Raymond and co-workers developed a water-soluble tetrahedron structure $K_{12}[Ga_4L_6]$ (L = *N*,*N*-bis(2,3-dihydroxybenzoyl)-1,5-diaminonaphthalene; Figure 1c) able to catalyze different reactions such as the hydrolysis of orthoformates,[23,24] aza-Cope rearrangement,[25] hydroalkylation,[26] Nazarov cyclization,[27] allyl alcohol isomerization,[28] reductive elimination from Au(III) and Pt(IV) complexes,[29−31] the Prins,[32,33] and the aza-Prins cyclization reactions.[34,35]

The Prins reaction, the subject of the present investigation, involves the formation of new carbon−carbon bonds achieved through the acid-catalyzed condensation of aldehydes with alkenes; it is a key point in the synthesis of terpenoids here considered.[32,33] Several computational studies have addressed the reaction mechanism for the Prins reaction.[36−39] In the present selected process, when performed in solution, citronellal **1o** (o denotes open conformation) is converted

Received: August 6, 2024
Revised: November 5, 2024
Accepted: November 18, 2024
Published: December 9, 2024

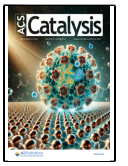

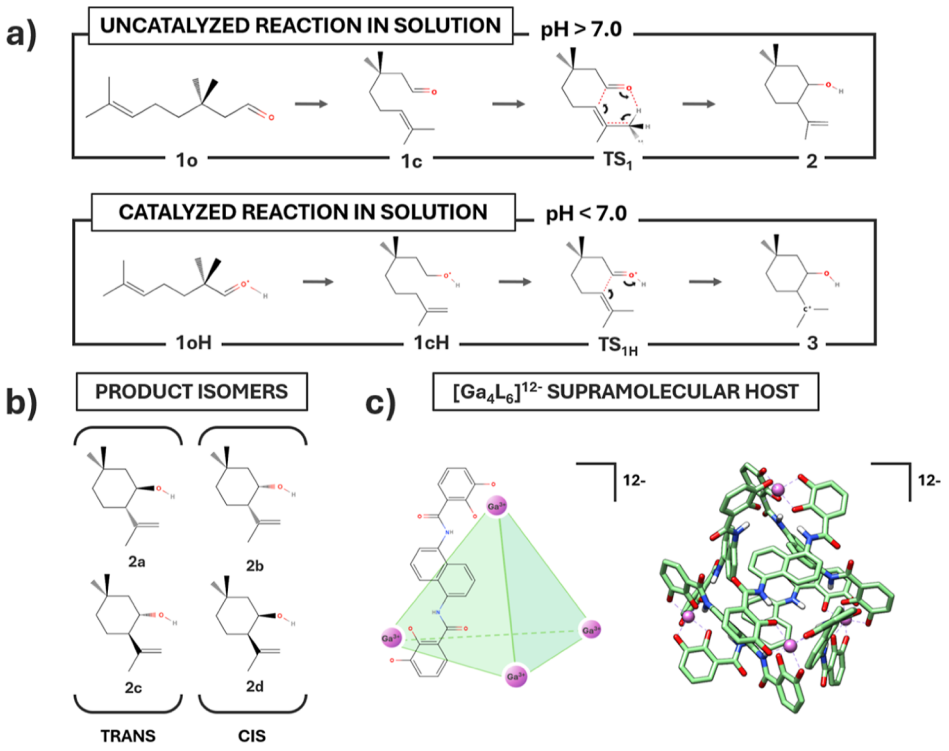

Figure 1. Schematic representation of the Prins reaction studied: (a) uncatalyzed and acid-catalyzed reactions; (b) product isomers; and (c) schematic representation of the $[Ga_4L_6]^{12-}$ metallocage.

into its protonated form **1oH** in acidic conditions (Figure 1a).[40] This protonated form undergoes cyclization by adopting first a closed conformation of the reactant, **1cH**, and then forming the carbocation intermediate **3**. From this intermediate, various products can be derived: two major products being *p*-menthane-3,8-diols and *p*-menthane-3,8-diol citronellal acetals, the latter formed by condensation with compound **1o**. Additionally, a mixture of alkene isomers is formed as minor products (**2a−d**; Figure 1b).[41]

Raymond, Bergman, Toste, and co-workers reported the cyclization of citronellal catalyzed by the $[Ga_4L_6]^{12-}$ metallocage under slightly basic conditions (pH 8.0).[41,42] They observed significant rate accelerations, ranging from 10^4 to 10^5 times faster compared to the uncatalyzed reaction, with the metallocage exhibiting one of the highest catalytic efficiencies observed for synthetic supramolecular cavities. In contrast to catalysis in acidic aqueous solutions, which predominantly yields diol products, the catalytic cage shows a higher selectivity for the formation of alkene isopulegol products **2** (Figure 1b); concretely, they observed the formation of **2a** (isopulegol) and **2b** (neoisopulegol) as the major products. This selectivity is particularly relevant as it emulates the behavior of natural terpene synthases, presenting a viable alternative for the synthesis of these monoterpene derivatives.[43,44] Additionally, the use of this catalytic metallocage induces a shift in the preference from cis to trans isomers.

Experimental studies suggest that in the presence of the metallocage, the reaction begins with the encapsulation of the substrate, a process that is reversible and rapid,[24,41,45] involving the displacement of solvent molecules from the host cavity by the substrate aldehyde.[46,47] The proposed mechanism suggests that after encapsulation, the host facilitates substrate **1** ⊂ **Δ** activation by stabilizing its conjugate acid, thereby promoting the protonation of the carbonyl oxygen, **1H** ⊂ **Δ**. According to this hypothesis, the reaction proceeds through a stepwise pathway postulated based on the characterization of the carbocation intermediate **3** (Figure 1a).[42] However, a prior conformational adaptation is essential for cyclization to take place, requiring the guest molecule to achieve a closed/proreactive configuration, **1cH** ⊂ **Δ**. Previous studies have shown that supramolecular hosts can induce a chair conformation in acyclic guests.[48−50] This is also proposed in the mechanistic study of the related aza-Prins reaction on the same metallocage performed by Xu and co-workers.[35] The present study aims to evaluate all of these reaction steps to identify the key factors governing the rate acceleration of this process.

To elucidate catalytic mechanisms at the molecular scale, in solution and inside the cavity, computational evaluation is undertaken.[51−53] Despite their significance, theoretical studies on rate-accelerated reactions within supramolecular hosts remain relatively limited,[54−63] although they have been increasing recently.[64−66] A combination of QM, QM/MM, and molecular dynamics (MD) simulations are presented to investigate the origin or rate acceleration of the Prins reaction on the selected citronellal reactant for the synthesis of terpenoids in the presence of the $[Ga_4L_6]^{12-}$ metallocage.

COMPUTATIONAL DETAILS

All DFT and DFT/MM calculations were conducted using the Gaussian 16 software package.[67] Geometry optimizations were performed using the B3LYP/6-31G(d,p) level of theory,[68,69] incorporating the D3 Grimme correction[70] for dispersion for the DFT and the high-level region of DFT/MM, while the low-level region employed the general Amber force field (GAFF2). Potassium counterions were not included in the low-level ONIOM calculations as they were not relevant for the model (vide infra and ref 31).[31] Electronic embedding was

https://doi.org/10.1021/acscatal.4c04696
ACS Catal. 2024, 14, 18722−18733

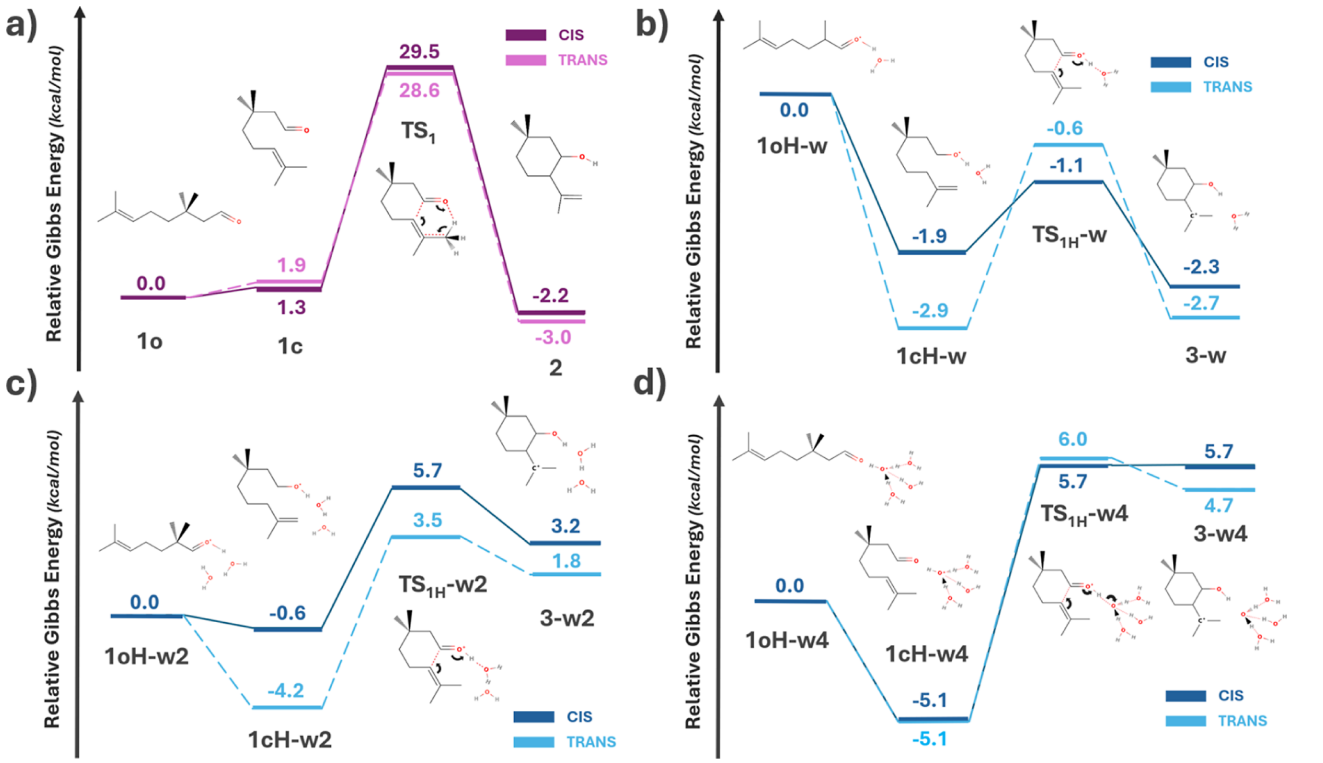

Figure 2. Gibbs energy profiles (T = 298 K) for the studied processes in solution: (a) neutral conditions and acidic conditions with (b) 1 explicit water molecule, (c) 2 explicit water molecules, and (d) 3 explicit water molecules.

enabled by the ONIOM=EmbedCharge option. For gallium, the SDD pseudopotential and associated basis set, supplemented with a set of d polarization functions, were utilized,[71,72] while the 6-31G(d,p) basis set was applied to all other atoms.[73] The geometries of reactants, intermediates, transition states, and products were optimized in an aqueous solvent using the CPCM continuum model.[74] Gibbs energies were calculated at 298 K. A correction of 1.9 kcal/mol was applied to each compound to change the standard state from the gas phase (1 bar) to solution (1 M).[75] These calculations contained systems of more than 300 atoms. Full QM calculations at the same level for the complete encapsulated system were performed for two selected Gibbs energy barriers to validate the ONIOM results.

MD simulations were conducted employing the AMBER 16 package (AmberTools16)[76] employing the CUDA version of the pmemd program. The MD simulation box size was 49 × 41 × 42 Å^3 and treated under periodic boundary conditions. The short-ranged nonbonded interactions were limited to a cutoff of 9 Å, while the long-ranged electrostatic terms were handled by the particle mesh Ewald (PME) method.[77] The simulated systems comprised the cage, the guest molecule, 11 or 12 potassium counterions to maintain overall neutrality, and explicit water solvent molecules modeled using the TIP3P model (around 1950 water molecules considered).[78]

During simulations, a constant temperature of 298.15 K was maintained through a Langevin thermostat, while pressure was maintained at 1 bar using a Monte Carlo barostat.[79] The force field parameters for the metallocage were taken from prior studies conducted by our research group.[80] Bonding parameters for the organic constituents of both host and guest molecules were adopted from the widely used general AMBER force field (GAFF2).[81]

Simulations of 1 μs were performed for systems representing reactants, intermediates, and products, both in bulk solution and confined within the metallocage. Subsequent clustering analysis identified key configurations, serving as initial coordinates for QM/MM investigations into reactivity. The binding Gibbs energies (ΔG_{bind}) were computed using the attach−pull−release (APR) method.[82,83]

The well-tempered adaptively biased molecular dynamics (WT-ABMD) simulations[84−87] were also performed using the CUDA version of the pmemd program of the AMBER 16 package.[76] The simulation box was the same as that described for the plain molecular dynamics simulations and treated under periodic boundary conditions. To keep constant temperature, 300 K, and pressure, 1 bar, the same thermostat and barostat as before were applied. A cutoff of 9 Å was used for nonbonded interactions, and long-range electrostatic interactions were accounted for by the PME method.[77] A time step of 2 fs was used, and the simulation time was 60 ns. The distance between the two carbon atoms involved in the cyclization was selected as a collective variable, and the resolution for the reaction coordinate was 0.2. The nfe-umbrella-slice utility was used to obtain the Gibbs energy profile.

RESULTS AND DISCUSSION

The results are presented in several sections. In the first section, the reaction in solution is evaluated. In the second section, there is a description of the analysis performed by means of classical molecular dynamics simulations to understand the behavior of encapsulated reactants inside the $[Ga_4L_6]^{12-}$ metallocage. The next section investigates the encapsulation process of the reactant (neutral and protonated) into the cavity of the metallocage. The last section analyzes the

https://doi.org/10.1021/acscatal.4c04696
ACS Catal. 2024, 14, 18722−18733

reaction mechanism within the metallocage by comparing the obtained results with those in solution.

Reaction in Solution. The Prins cyclization of citronellal is catalyzed in an acidic medium through the activation (protonation) of the reactant. Although the predominant reaction under these conditions results in the formation of diol products, for comparative purposes, our study focuses on the alkene that is the product obtained in the presence of the cage.[42] Therefore, the reaction profiles presented in this section are centered to mimic the host−guest catalytic reaction in bulk solution.

First, we examined the nonacidic, uncatalyzed reaction of citronellal **1** in bulk solution, focusing exclusively on the alkene production. This reaction involves an intramolecular cyclization without reactant activation, assuming that the medium is neutral (or slightly basic). The process occurs in a concerted manner, where the closure of the C−C bond via electrophilic addition of the aldehyde and the proton displacement take place simultaneously (TS_1, Figure 1a). The obtained isopulegol products (**2**) can be categorized into four isomers: isopulegol (**2a**), neoisopulegol (**2b**), isoisopulegol (**2c**), and neoisoisopulegol (**2d**); see Figure 1b. Studies by Raymond, Bergman, Toste, and co-workers have identified **2a** and **2b** as the predominant products, with conversions of 52% and 32%, respectively.[42] Therefore, our computational study centers on these primary configurations, designated as trans (**2a**) and cis (**2b**), reflecting the relative orientation of the aldehyde and isopropyl groups (configuration shown in Figure 1b).

By employing DFT calculations, we determined that the cyclization barrier for compound **1** results in a relative Gibbs energy barrier of 29.5 kcal/mol for the cis product and 28.6 kcal/mol for the trans product (Figure 2a). This is consistent with the experimentally reported activation Gibbs energy of $\Delta G^{\ddagger}_{exp}$ = 27.3 kcal/mol for uncatalyzed cyclization under pH = 8.0 and 25 °C, extracted from the measured rate constant of 5.7×10^{-8} s^{-1}.[42] This shows close agreement between the computational values and experimental results. Furthermore, the Supporting Information includes considerations on model benchmarks (Figures S8 and S9).

Following the mechanism suggested by Raymond and coworkers, we explored the catalyzed reaction where the activated citronellal compound, in an acidic medium, undergoes protonation and cyclization of **1o**, resulting in the carbocation intermediate **3**. We assume that a charged hydronium ion acts as the proton source for the **1o** → **1oH** activation. As our objective is also to emulate the reaction taking place inside the cavity, considering the presence of additional water molecules assisting the hydronium ion might be relevant as they can influence its proton-donating capabilities. Therefore, we evaluated the cyclization process considering a different number of explicit solvent molecules (depicted in Figure 2): (b) a single hydronium ion, (c) a hydronium ion assisted by one additional water molecule, and (d) a water cluster where the hydronium ion is assisted by three extra water molecules. Although the last situation cannot occur inside the guest cavity (vide infra), it may better represent the acid-catalyzed reaction in bulk solution.

The results indicate an increasing energy barrier for the cyclization process as more water molecules assist the donor hydronium ion. Specifically, we observe barriers around 1−2 kcal/mol for case (b), approximately 6−8 kcal/mol for case (c), and around 11 kcal/mol for case (d), considering both cis and trans configurations. This trend shows that the presence of explicit surrounding water clusters around a hydronium ion reduces its acidity; the extensive hydrogen bonding network stabilizes the proton, making it less likely to be donated. In less hydrated environments, such as within the hydrophobic cavity of a host−guest complex, the hydronium ion is more likely to donate a proton, enhancing its acidic capability. Although MD results indicate a recurring presence of two water molecules inside the cavity (vide infra), we do not expect similarities with case (c) as clustering positions show that the configuration inside the metallocage maintains both water molecules separated, impeding solvation shielding (see Figure S12). Therefore, the configuration inside the cavity should be closer to the scenario of the isolated hydronium molecule observed in case (b).

The fully solvated hydronium ion, case (d), which exhibits higher activation barriers, corresponds to the situation that more accurately represents catalysis in an acidic solution in the absence of a supramolecular catalyst. However, its significance is relative upon recognizing that such a pathway to alkene production after cyclization should be less favored compared to diol production, that is, the one observed experimentally but not studied here.

The process studied experimentally is performed under neutral or slightly basic conditions and in the presence of the metallocage. The Gibbs energy barrier for the uncatalyzed process is 27.3 kcal/mol. The experimentally measured decrease of Gibbs energy barrier by the presence of the metallocage is −5.7 kcal/mol.[42] Therefore, the Gibbs energy barrier for the process in the presence of the metallocage should be 21.6 kcal/mol. Calculations show that an isolated hydronium could induce cyclization with a barrier lower than 2 kcal/mol, as observed in case (b), Figure 2b; thus, considering an isolated hydronium ion inside the cavity, it should give similar values. Therefore, the remaining energy requirements likely arise from other aspects of host−guest catalysis. These should include the encapsulation process, protonation/activation of the substrate, and conformational closing of the guest inside the cavity. Next sections will focus on exploring these steps to identify the requirements beyond the decrease in the barrier.

Host−Guest Behavior: Reactant Conformation and Solvent Availability. Prior to the investigation of the catalytic reaction process, it is important to analyze the behavior of the reactants encapsulated in the metallocage, including its conformational arrangement within the cavity, as well as the solvent's role in the system. Given the activation (protonation) requirement of **1** for the catalytic reaction to occur, the importance of water availability inside the metallocage becomes evident. Therefore, analyzing the dynamic evolution of encapsulated solvent molecules along with the reactant is necessary. Additionally, we aimed to assess the cage's ability to accommodate the guest reactant in its open (**1o**) and closed (**1c**) conformations, the latter potentially conducive to cyclization. To achieve these objectives, classical molecular dynamics (MD) simulations along with enhanced sampling ABMD method of the unprotonated (**1**) and protonated (**1H**) guests were performed in explicit solvent and encapsulated inside the $[Ga_4L_6]^{12-}$ metallocage, both in a periodic box of explicit water molecules.

The distance between C−C atoms involved in the cyclization was analyzed over a 1 μs MD trajectory in a water solution. This C−C distance served as an indicator of the conformation, considered closed under 4 Å and open for larger

https://doi.org/10.1021/acscatal.4c04696
ACS Catal. 2024, 14, 18722−18733

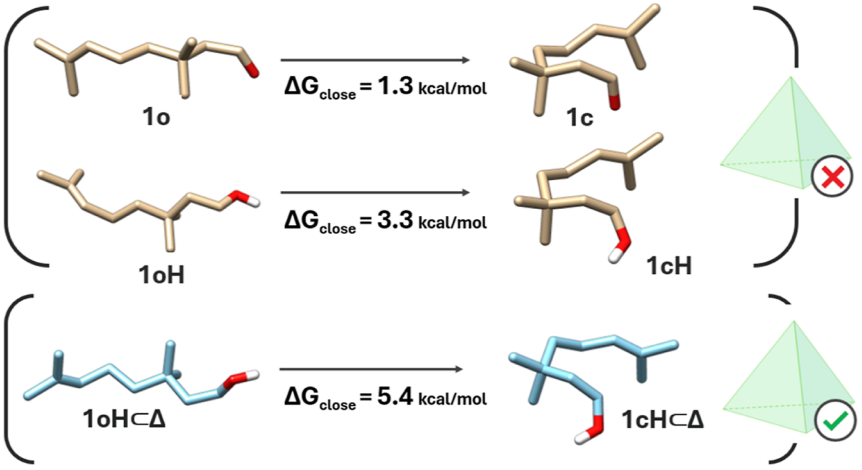

Figure 3. Gibbs energy comparison for the open and closed conformations of the reactant in solution and within the cavity of the metallocage.

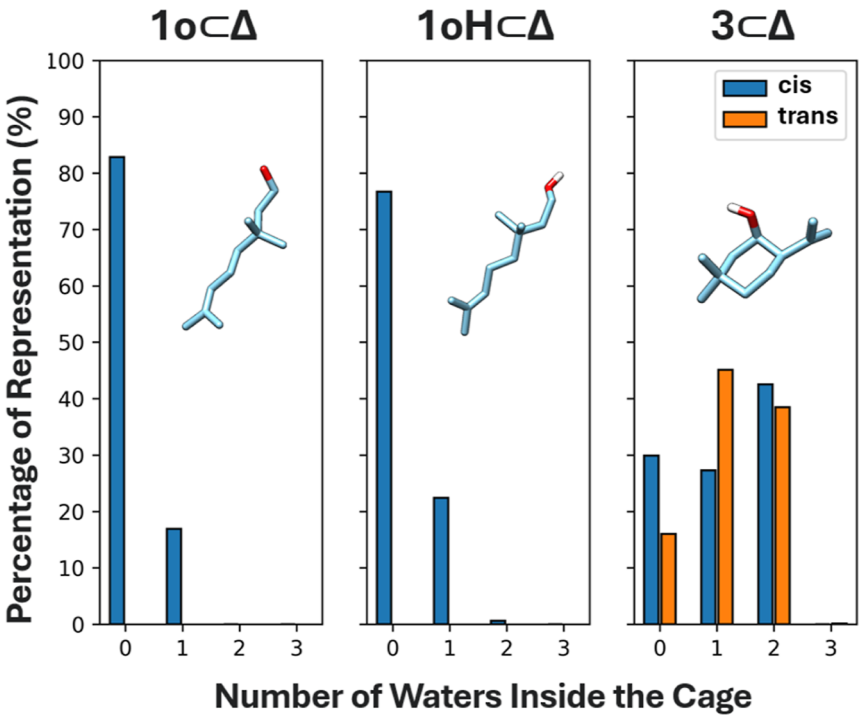

Figure 4. Evaluation of the presence of solvent molecules inside the cavity of the $[Ga_4L_6]^{12-}$ metallocage along with the guest in their neutral, **1o** ⊂ **Δ**, protonated, **1oH** ⊂ **Δ**, and cyclized, **3** ⊂ **Δ**, forms.

values. The MD simulation in explicit solvent reveals that both conformations are accessible for unprotonated (**1**) and protonated (**1H**) forms. However, for both neutral and protonated states, the open conformation is much more visited throughout the molecular dynamic simulations, with average C−C distances of 5.2 and 5.0 Å, respectively (see Figure S1). For the encapsulated unprotonated guest (**1** ⊂ **Δ**), the closed conformation is never observed; moreover, during the MD simulation, the guest is expelled from the cavity (see Figure S2). For the protonated guest (**1H** ⊂ **Δ**), the closed conformation is not observed either, but it remains within the cavity for 1 μs MD simulation time. This indicates the metallocage's inability to enforce a more compact and closed conformation of the reactant within the cavity.

To further validate these findings, we performed a conformational analysis for the substrate in solution and calculated the Gibbs energy difference between the closed and open conformations for both unprotonated (**1**) and protonated (**1H**) reactants (Figure 3). In solution, the closed conformation is calculated to be 1.3 and 3.3 kcal/mol higher than the lowest-energy open conformation for the unprotonated and protonated substrates, respectively. Then, we investigated the conformational change of the substrate when encapsulated in the cage. From the classical MD simulations, we observed that the unprotonated guest (**1** ⊂ **Δ**) prefers to be in solution rather than in the cage (Figure S2). Therefore, we calculated the relative Gibbs energy of the conformational change for the protonated substrate inside the metallocage (**1oH** ⊂ **Δ**). To do that, we employed the distance between the two carbon atoms involved in the new-forming C−C bond in the cyclization as a collective variable for the well-tempered adaptively biased molecular dynamics (WT-ABMD) simu-

https://doi.org/10.1021/acscatal.4c04696
ACS Catal. 2024, 14, 18722−18733

lation. The simulation revealed that the pro-reactive form (**1cH** ⊂ **Δ**) is 5.4 kcal/mol higher in energy compared to the lowest-energy open conformation (Figure 3).

Notably, this observation aligns with the molecular dynamics results where the system spontaneously evolves to the open conformation; thus, reactant preorganization (forming the closed conformation) is not favored. Indeed, contrary to what is generally expected and to what was observed for other reactants within supramolecular cages,[88] the host in this case hinders rather than facilitates the closure of the guest molecule when compared to the process in solution. To further investigate these results, we performed additional MD analyses comparing the trajectory of the close conformation (by constraining the C−C cyclization distance) to that of the open form (see Figures S3 and S4). For the open conformation, the positive part of the reactant (the protonated C═O group) forms a hydrogen bond with the partially negatively charged corner of the cage (oxygens from the catechol groups). Such hydrogen bonds are not observed for the close conformation along the trajectory. This suggests that breaking this hydrogen bond is necessary for the guest to adopt the close conformation, mostly accounting for the additional energy required to close the guest inside the cage. The nature of the interactions between the positive part of the reactant and the corners of the metallocage were also identified by Xu and co-workers.[35]

To evaluate the presence of water molecules within the cavity, a custom-developed script was employed to track the number of water molecules entering the tetrahedral volume defined by the four gallium vertices in each frame.[88] The host−guest complexes with the open guest conformations (**1o** ⊂ **Δ** neutral and **1oH** ⊂ **Δ** protonated) show a significant absence of water molecules throughout most of the trajectory (Figure 4). For the neutral one, **1o** ⊂ **Δ**, a single water molecule appears in 16.9% of the frames, whereas no water molecules are observed for 83% of the frames. For the protonated substrate, **1oH** ⊂ **Δ**, these percentages are 22.5% and 76.9%, respectively. The presence of two or three water molecules is only occasionally observed. This indicates a lack of available space inside the cavity, when the guest is in its open form. Due to the energetic cost associated with adopting a closed conformation, it is likely that the guest is activated through protonation while still in its open form. Thus, the presence of at least one water molecule is crucial for this process, as is in fact observed for the neutral (16.9% occurrence) and protonated guests (22.5% occurrence), respectively.

In addition to these analyses, cyclizated intermediate **3** was also subjected to molecular dynamics simulations in its encapsulated form (**3** ⊂ **Δ**) to monitor the position, flexibility of the guest, and water availability inside the cavity. Both cis and trans configurations, formed after the cyclization, were considered in the calculations, with chair conformations assumed to be the most stable forms (Figure 4). As expected, the more compact guest structure **3**, in its cis and trans isomers, allowed for greater water molecule encapsulation, with occurrences of 30% and 16% for zero water molecules, 45.2% and 27.4% for one water molecule, and occurrences of 38.6% and 42.6% for two water molecules, respectively. These results suggest that for a more enclosed guest conformation, additional space is available, allowing a second water molecule to enter the cavity. Moreover, we consistently observe a water molecule anchored to the guest's alcohol group and oriented toward a cage vertex throughout the trajectories (Figure S5).

The obtained trajectories were subjected to clustering analysis to identify the most frequently occurring positions, thereby capturing the most relevant scenarios throughout the simulations. Among all studied systems, particular emphasis was placed on the positions of the guest and the explicit water molecules inside the cage. However, as previously mentioned, the cage's inability to induce guest closed conformations made the clustering analysis of **1cH** ⊂ **Δ** involved in the cyclization reaction unfeasible. For this reason, clustered poses of intermediate **3** ⊂ **Δ** were taken as references for the host-catalyzed system, which consistently showed the presence of two water molecules inside the cavity as the most frequently observed configuration. These clustered final positions, including two explicit waters, were considered for reactivity studies (in both solution and inside the cavity), ensuring consistency with the observed orientations in host−guest dynamics.

Supplementary analyses were also conducted on the MD simulations to examine cage movement and geometry distortion, cavity volume evolution, and overall stability. By tracking Ga−Ga distances between the cage vertices and ligand angles, we observed that the cage maintained a highly stable structure with no distortion in its tetrahedral geometry (see Figures S6 and S7), consistent with previous works.[89] The cavity volume was measured for each frame using the *fpocket* software,[90,91] both with and without the guest molecule. The results align with volumes reported in previous studies, ranging from 250 to 320 Å^3, with a standard deviation around 24 Å^3 for open conformations of the substrate and around 18 Å^3 for the cyclizated ones (see Figures S8 and S9).[88] The empty cage exhibited a similar volume, although with a higher deviation. This suggests that the encapsulated guest molecule contributes to stabilizing the cage movement, to some extent. However, given the stability of the cage's tetrahedral geometry, the volume differences may be primarily attributed to the orientation of the naphthalene of the linker groups. In the absence of a guest, these naphthalenes exhibit greater degrees of freedom, leading to more significant volume variations. Additionally, the presence of the citronellal guest induces a slight contraction of the cage, consistent with previous literature reports comparing host−guest complex volumes to those from the unoccupied cage.[35]

It is also worth noting that MD simulations for the **1o** ⊂ **Δ** complex revealed that the unprotonated guest is consistently ejected from the cage across all of the performed dynamics (three replicas). In contrast, the **1oH** ⊂ **Δ** complex, containing the protonated guest, remains stably encapsulated within the cage. This last scenario likely occurs due to stabilizing electrostatic interactions of the cationic guest with the cage environment. The observed dissociation of the unprotonated guest evidence a low binding energy barrier for its entrapment by the cage. The implications of this finding will be discussed in greater detail in a subsequent section on host encapsulation.

Host−Guest Encapsulation and Guest Protonation. Host−guest encapsulation plays a crucial role in understanding the catalytic processes of supramolecular cages. This phenomenon involves the trapping of guest molecules within the internal cavities of host structures, which can significantly alter the reactivity and stability of the encapsulated species. Specifically, for the cationic guest **1oH** ⊂ **Δ**, electrostatic interactions with the negatively charged host enhance the binding process. To analyze whether activation of **1o** precedes or follows encapsulation, we studied the binding for both

https://doi.org/10.1021/acscatal.4c04696
ACS Catal. 2024, 14, 18722−18733

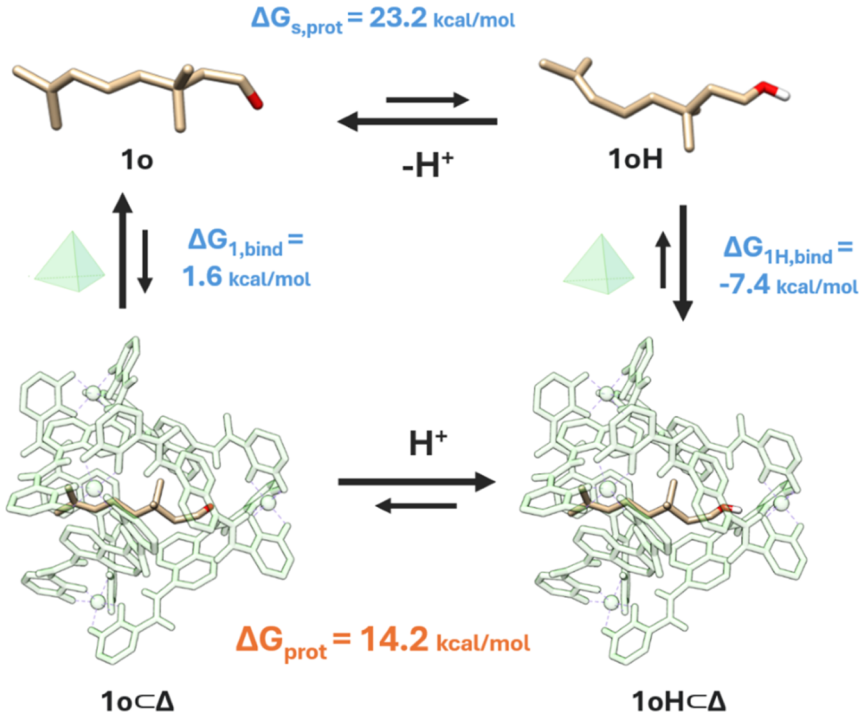

Figure 5. Thermodynamic cycle employed to determine ΔG_{prot} of the encapsulated reactant.

unprotonated **1o** and protonated **1oH** guests. It is expected that under experimental reaction conditions the metallocages are occupied with the substrate (the concentration of the reactant is much larger than that of the metallocages).[41,42] The encapsulation process was calculated employing a protocol we recently established for calculating Gibbs binding energies (ΔG_{bind}) in supramolecular metallocages using the attach−pull−release (APR) method[83,84] (see Computational Details). The values for the binding Gibbs energies show that the encapsulation of unprotonated guest **1o** is 1.6 ± 0.7 kcal/mol, while that of protonated **1oH** is −7.4 ± 0.9 kcal/mol. These results reveal the spontaneous nature of trapping a cationic guest, driven by electrostatic effects. Conversely, the binding of the neutral (unprotonated) **1o** exhibits a low energetic requirement, aligning with the observed MD behavior, where the unprotonated guest tends to dissociate from the host.

To analyze whether protonation takes place in solution or inside the metallocage, the ΔG_{prot} of protonation in both environments needs to be computed. In solution, $\Delta G_{s,prot}$ is calculated using a standard protocol for obtaining pK_a based on DFT methods applied to a stablished thermodynamic cycle[75,92−94] (see Figure S11); the obtained value is $\Delta G_{s,prot}$ = 23.2 kcal/mol. Once encapsulated, computing ΔG_{prot} of a neutral substrate is challenging due to the intricate nature of determining such Gibbs energy within the metallocage. The thermodynamic cycle employed in solution cannot be applied here because it requires the Gibbs energy for the solvation of the encapsulated proton (from the gas phase to encapsulated in solution), a value that is not reliably obtained through continuum methods. As an alternative, we calculated the Gibbs energy difference (ΔG_{prot}) between the protonated and nonprotonated substrates inside the metallocage using the thermodynamic cycle shown in Figure 5. In this framework, the Gibbs energy relationship for protonating the neutral substrate in solution ($\Delta G_{s,prot}$) and inside the metallocage (ΔG_{prot}) must correspond to the relationship between the Gibbs energies for encapsulating both the neutral ($\Delta G_{1,bind}$) and protonated ($\Delta G_{1H,bind}$) substrates.

The binding Gibbs energies for two steps in the thermodynamic cycle, $\Delta G_{1,bind}$ and $\Delta G_{1H,bind}$, previously denoted, are 1.6 and −7.4 kcal/mol, respectively. Additionally, the Gibbs energy barrier for protonating the substrate in solution, $\Delta G_{s,prot}$, is 23.2 kcal/mol. Assuming that these ΔG values can be combined despite being obtained through different computational approaches, the calculated Gibbs energy for the protonation of the encapsulated neutral substrate, ΔG_{prot}, is 14.2 kcal/mol (Figure 5). The basicity of the citronellal reactant is significantly modified once encapsulated.

Based on these analyses, the results suggest that guest protonation occurs inside the host cavity after encapsulation. Protonation in solution has a $\Delta G_{s,prot}$ of 23.2 kcal/mol, a value clearly higher than 15.8 kcal/mol obtained by adding encapsulation ($\Delta G_{1,bind}$ = 1.6 kcal/mol) and protonation of the reactant inside the metallocage (ΔG_{prot} = 14.2 kcal/mol). This finding is consistent with the neutral/basic conditions of the surrounding solvent. According to these results, for studying the cyclization process in the next section, we solely consider the protonated reactant within the cage.

The protonation process highlights the cage's ability to catalyze what is traditionally an acid-catalyzed reaction but under neutral conditions. This shows that the cage is able to create a "low pH" environment within the cavity,[95] as proposed by Warshel et al. for hydrolysis of orthoformates using the same $[Ga_4L_6]^{12-}$ metallocage. Indeed, according to the thermodynamic cycle shown in Figure 5, the Gibbs energy for the protonation step is 9.0 kcal/mol more favorable inside the cage than in solution. The pronounced change in the basicity of the aldehyde upon encapsulation is crucial for accelerating the reaction. A similar behavior was also observed for the Nazarov cyclization within the same metallocage.[88,96]

https://doi.org/10.1021/acscatal.4c04696
ACS Catal. 2024, 14, 18722−18733

Reaction inside the Metallocage. In previous sections, we presented classical molecular dynamics simulations of the host−guest in a periodic box of explicit solvents for encapsulated intermediate **3-w2** ⊂ **Δ**. The most representative structures after clustering the frames reported a consistent presence of two water molecules inside the cage. Thus, for calculating the Gibbs energy profile at the QM/MM level for the cyclization step, we selected the most representative structures for both isomers, cis **3c-w2** ⊂ **Δ** and trans **3t-w2** ⊂ **Δ**. We analyzed the mechanism backward to identify the reaction profile for the cyclization step. The QM region includes the protonated substrate in the closed conformation and two water molecules altogether in the cavity of the $[Ga_4L_6]^{12-}$ metallocage. The MM region includes the supramolecular cage.

The **TS_{1H}-w2** ⊂ **Δ** transition state for substrate cyclization, involving two water molecules, reveals a relative Gibbs energy barrier of $\Delta G^{\ddagger}$ = 0.7 kcal/mol in the optimal scenario, corresponding to the trans configuration. For the case of the cis isomer, the relative Gibbs energy barrier is $\Delta G^{\ddagger}$ = 2.1 kcal/mol; additional configurations were optimized with similar but higher relative energy barriers ($\Delta G^{\ddagger}$ of 3.3, 3.8, and 5.1 kcal/mol, respectively). These results show a cis−trans selectivity that aligns very well with experimental data. Additionally, DFT optimizations of the reactant, transition states, and products were performed for the entire model at full QM level to compare with ONIOM calculations. The calculated energy barriers obtained were 2.5 and 4.2 kcal/mol for the trans and cis steps, respectively; these values validate the use of ONIOM calculations for this system. The optimized geometries for the cis and trans transition states of the encapsulated substrate along with two explicit water molecules are shown in Figure 6.

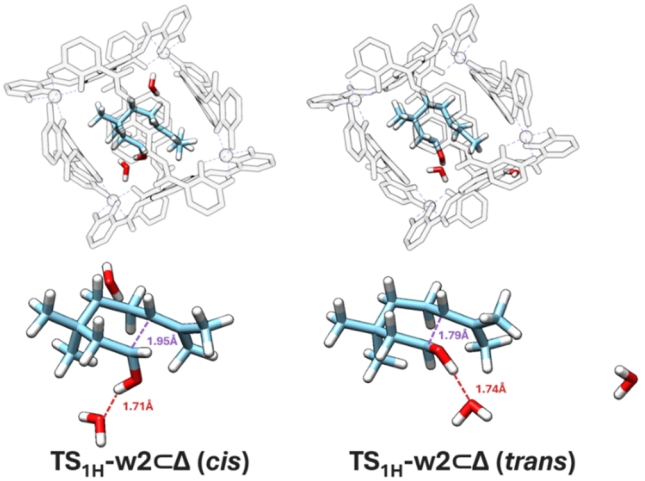

Figure 6. Optimized geometry of the transition states for the cis and trans pathways; they are shown isolated and inside the metallocage.

The effect of the presence of K^+ ions surrounding the $[Ga_4L_6]^{12-}$ metallocage on the Gibbs energy barrier was also evaluated. We calculated the Gibbs energy barrier for the trans configuration including 7 K^+ because this is the average number of K^+ ions surrounding the $[Ga_4L_6]^{12-}$ metallocage in solution.[97] The Gibbs energy barrier with and without considering K^+ counterions is 0.4 and 0.7 kcal/mol, respectively, showing that the number of counterions surrounding the metallocage does not significantly influence the Gibbs energy barrier. A similar observation was obtained in a previous related investigation on this metallocage.[31]

The overall reaction profile for the mechanism inside the metallocage is shown in Figure 7. The first step involves encapsulation of the neutral reactant with a Gibbs energy of 1.6 kcal/mol. The Gibbs energy cost for protonating the reactant inside the cavity, calculated in a previous section, is 14.2 kcal/mol. For the reaction to proceed, the reactant must undergo a conformational change from the open to the closed conformation, with an associated energy cost of 5.4 kcal/mol, also calculated previously. For the subsequent cyclization step, where a new C−C bond is formed, we performed QM/MM calculations. The QM level region includes the reactant and several solvent molecules, as previously denoted.

Experimental investigation of the host-catalyzed reaction reported a barrier of 21.6 kcal/mol, whereas in solution it is 27.3 kcal/mol.[42] Thus, experimental evidence of $[Ga_4L_6]^{12-}$ activity indicates a decrease in the Gibbs energy barrier of 5.7 kcal/mol. Through computational analysis, we determined that the host-catalyzed reaction has an overall Gibbs energy barrier of 21.9 kcal/mol (in its most favorable trans isomer), substantially lower than the uncatalyzed barrier of 28.6 kcal/mol. This corresponds to a decrease in the Gibbs energy barrier of 6.7 kcal/mol. On the other hand, the cis isomer has an overall barrier of 23.3 kcal/mol, indicating a decrease of 6.2 kcal/mol compared to the reference barrier of 29.5 kcal/mol for the unprotonated cis form. These results demonstrate excellent concordance between the theoretical predictions and experimental results. Moreover, they also show that within the metallocage, the change in basicity of the reactant significantly facilitates the reaction, whereas conformational preorganization hinders the process, conversely to what is generally expected.

CONCLUSIONS

The reaction mechanism for the Prins cyclization of citronellal was analyzed both in solution and within the $[Ga_4L_6]^{12-}$ supramolecular cage. In solution, the computed mechanism varies by the presence or absence of hydronium ions, i.e., the pH of the solvent. Under basic or neutral conditions, the reaction proceeds via a one-step transition state involving intramolecular cyclization without prior reactant activation. In acidic conditions, however, protonation of citronellal leads to the formation of a carbocation intermediate, which subsequently forms alkene isopulegol products. Although the predominant product in solution is diol rather than the alkene,[42] utilizing the $[Ga_4L_6]^{12-}$ cage as a guest catalyst selectively favors alkene production over diol formation, similar to the biological activity of terpene synthases. Thus, this mechanism is the one compared in solution and within the metallocage.

For the process inside the cavity, the behavior of the system (metallocage, reactant, and water solvent) was analyzed using molecular dynamics simulations. The $[Ga_4L_6]^{12-}$ cage maintains a highly stable structure during simulations, with negligible distortion of its tetrahedral geometry. The guest molecules influence the cage's volume and stability, particularly in their orientation and the interaction of naphthalene groups. As far as the binding of reactant is concerned, the MD simulation shows that the neutral reactant **1** tends to be expelled from the metallocage, suggesting a low binding energy and weak interaction with the cage; this is in concordance with the computed ΔG_{bind} for **1** of 1.6 ± 0.7 kcal/mol. In contrast, protonated guest **1H** remains stably encapsulated during the

https://doi.org/10.1021/acscatal.4c04696
ACS Catal. 2024, 14, 18722−18733

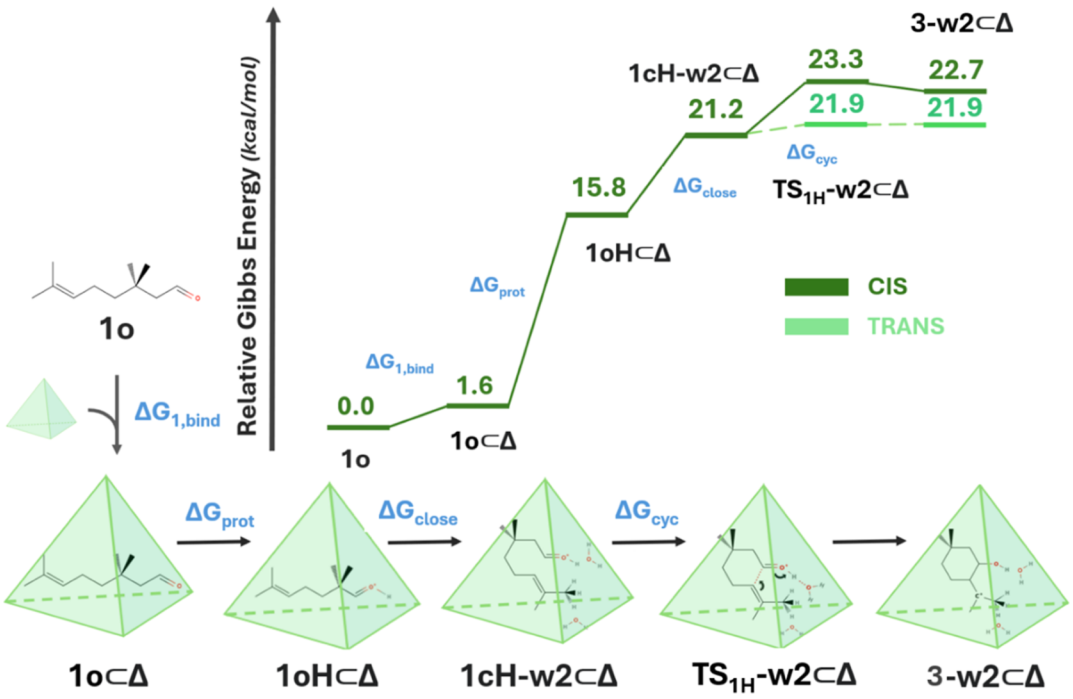

Figure 7. Gibbs energy profile for the Prins reaction inside the $[Ga_4L_6]^{12-}$ metallocage.

MD simulation, in agreement with the computed ΔG_{bind} of −7.4 ± 0.9 kcal/mol.

Protonation of the reactant is crucial for the catalytic process, and the presence of at least one water molecule inside the metallocage facilitates this protonation. The MD simulations show that on average, there are two water molecules along with the citronellal reactant inside the cavity. One of these water molecules is assumed to be a hydronium ion, serving as the proton donor for guest activation. This assumption is supported by studies indicating a low "local pH" inside the cavity of this metallocage.[95] The protonation of the guest within the metallocage is energetically more favorable (ΔG_{prot} = 14.2 kcal/mol) compared to protonation in solution ($\Delta G_{s,prot}$ = 23.2 kcal/mol). This reveals that the change in basicity of the reactant inside the cage is crucial for the rate acceleration process and is behind the acceleration process.

The encapsulated reactant in the metallocage predominantly adopts an open conformation, both in unprotonated **1** and protonated **1H** forms. Indeed, conformational analysis for the protonated form shows that the open conformation, **1oH**, is more favorable than the closed conformation, **1cH**, by 5.4 kcal/mol. Therefore, conversely to what is generally assumed in cyclization processes within metallocages, the cavity does not facilitate the formation of a more compact conformation needed to undertake the cyclization. Therefore, the preorganization effect of metallocage cavities cannot be as general as expected. Finally, the results indicate very low relative Gibbs energy cyclization barriers of 0.7 and 2.1 kcal/mol for trans and cis pathways, respectively, consistent with the results obtained in the acid-catalyzed reaction in a solvent.

The overall barrier for cis and trans configurations (23.3 and 21.9 kcal/mol, respectively) is significantly lower than that of the uncatalyzed reaction (29.5 and 28.6 kcal/mol). Note that the overall encapsulated reaction involves the following steps with their energetic requirements: (i) guest encapsulation, (ii) guest protonation, (iii) guest conformational closing to adopt a pro-reactive disposition, and (iv) cyclization. Importantly, we identified novel factors governing the reactivity as the change of basicity of the guest upon encapsulation, becoming crucial for the process, and the fact that the $[Ga_4L_6]^{12-}$ cage does not promote a more compact conformation of the citronellal guest facilitating the cyclization; this is in contrast with previous reports involving other hosts and different guests within the same cage. These new findings are relevant to the future development of metallocages as a catalyst.

■ ASSOCIATED CONTENT

Supporting Information

The Supporting Information is available free of charge at https://pubs.acs.org/doi/10.1021/acscatal.4c04696.

Open/closed conformation analysis in solution and within the metallocage; behavior of the cyclated intermediate within the cage; $[Ga_4L_6]^{12-}$ cavity and stability analysis with MD; benchmarks for the model; thermodynamic cycle for calculating $\Delta G_{s,prot}$; force field parameters; and cartesian coordinates (PDF)

■ AUTHOR INFORMATION

Corresponding Author

Gregori Ujaque − *Departament de Química and Centro de Innovación en Química Avanzada (ORFEO−CINQA), Universitat Autònoma de Barcelona, Barcelona 08193 Catalonia, Spain;* orcid.org/0000-0001-5896-9998; Email: gregori.ujaque@uab.cat

Authors

Iker Zapirain-Gysling − *Departament de Química and Centro de Innovación en Química Avanzada (ORFEO−CINQA), Universitat Autònoma de Barcelona, Barcelona 08193 Catalonia, Spain;* orcid.org/0000-0001-5117-7082

Gantulga Norjmaa − *Departament de Química and Centro de Innovación en Química Avanzada (ORFEO−CINQA),*

https://doi.org/10.1021/acscatal.4c04696
ACS Catal. 2024, 14, 18722−18733

Universitat Autònoma de Barcelona, Barcelona 08193 Catalonia, Spain

Jean Didier Maréchal − *Departament de Química and Centro de Innovación en Química Avanzada (ORFEO−CINQA), Universitat Autònoma de Barcelona, Barcelona 08193 Catalonia, Spain;* orcid.org/0000-0002-8344-9043

Complete contact information is available at: https://pubs.acs.org/10.1021/acscatal.4c04696

Notes

The authors declare no competing financial interest.

■ ACKNOWLEDGMENTS

Grants PID2020-116861GB-I00 and PID2023-150881NB-I00 funded by MCIN/AEI/10.13039/501100011033 are acknowledged. I.Z-G thanks the support from the grant PRE2021-098376.

■ REFERENCES

(1) *Supramolecular Catalysis: New Directions and Developments*; van Leeuwen, P. W. N. M., Raynal, M., Eds., Wiley, 2022.

(2) Yoshizawa, M.; Klosterman, J. K.; Fujita, M. Functional Molecular Flasks: New Properties and Reactions within Discrete, Self-Assembled Hosts. *Angew. Chem., Int. Ed.* **2009**, *48* (19), 3418−3438.

(3) Cook, T. R.; Stang, P. J. Recent Developments in the Preparation and Chemistry of Metallacycles and Metallacages via Coordination. *Chem. Rev.* **2015**, *115* (15), 7001−7045.

(4) Saha, R.; Mondal, B.; Mukherjee, P. S. Molecular Cavity for Catalysis and Formation of Metal Nanoparticles for Use in Catalysis. *Chem. Rev.* **2022**, *122* (14), 12244−12307.

(5) Holliday, B. J.; Mirkin, C. A. Strategies for the Construction of Supramolecular Compounds through Coordination Chemistry. *Angew. Chem., Int. Ed.* **2001**, *40* (11), 2022−2043.

(6) Han, M.; Engelhard, D. M.; Clever, G. H. Self-Assembled Coordination Cages Based on Banana-Shaped Ligands. *Chem. Soc. Rev.* **2014**, *43* (6), 1848−1860.

(7) Cook, T. R.; Zheng, Y.-R.; Stang, P. J. Metal−Organic Frameworks and Self-Assembled Supramolecular Coordination Complexes: Comparing and Contrasting the Design, Synthesis, and Functionality of Metal−Organic Materials. *Chem. Rev.* **2013**, *113* (1), 734−777.

(8) Ballester, P.; Fujita, M.; Rebek, J. Molecular Containers. *Chem. Soc. Rev.* **2015**, *44* (2), 392−393.

(9) Ibáñez, S.; Poyatos, M.; Peris, E. N-Heterocyclic Carbenes: A Door Open to Supramolecular Organometallic Chemistry. *Acc. Chem. Res.* **2020**, *53* (7), 1401.

(10) Ham, R.; Nielsen, C. J.; Pullen, S.; Reek, J. N. Supramolecular Coordination Cages for Artificial Photosynthesis and Synthetic Photocatalysis. *Chem. Rev.* **2023**, *123* (9), 5225−5261.

(11) Pullen, S.; Clever, G. H. Mixed-Ligand Metal−Organic Frameworks and Heteroleptic Coordination Cages as Multifunctional Scaffolds—A Comparison. *Acc. Chem. Res.* **2018**, *51* (12), 3052−3064.

(12) Bassani, D. M.; Darcos, V.; Mahony, S.; Desvergne, J.-P. Supramolecular Catalysis of Olefin [2 + 2] Photodimerization. *J. Am. Chem. Soc.* **2000**, *122* (36), 8795−8796.

(13) Gianneschi, N. C.; Bertin, P. A.; Nguyen, S. T.; Mirkin, C. A.; Zakharov, L. N.; Rheingold, A. L. A Supramolecular Approach to an Allosteric Catalyst. *J. Am. Chem. Soc.* **2003**, *125* (35), 10508−10509.

(14) Yoshizawa, M.; Klosterman, J. K.; Fujita, M. Functional Molecular Flasks: New Properties and Reactions within Discrete, Self-Assembled Hosts. *Angew. Chem., Int. Ed.* **2009**, *48* (19), 3418−3438.

(15) Hooley, R. J.; Rebek, J. Chemistry and Catalysis in Functional Cavitands. *Chem. Biol.* **2009**, *16* (3), 255−264.

(16) Breiner, B.; Clegg, J. K.; Nitschke, J. R. Reactivity Modulation in Container Molecules. *Chem. Sci.* **2011**, *2* (1), 51−56.

(17) Pemberton, B. C.; Raghunathan, R.; Volla, S.; Sivaguru, J. From Containers to Catalysts: Supramolecular Catalysis within Cucurbiturils. *Chem.—Eur. J.* **2012**, *18* (39), 12178−12190.

(18) Blaszkiewicz, C.; Bricout, H.; Léonard, E.; Len, C.; Landy, D.; Cézard, C.; Djedaïni-Pilard, F.; Monflier, E.; Tilloy, S. A Cyclodextrin Dimer as a Supramolecular Reaction Platform for Aqueous Organometallic Catalysis. *Chem. Commun.* **2013**, *49* (62), 6989−6991.

(19) Zhang, Q.; Tiefenbacher, K. Hexameric Resorcinarene Capsule Is a Brønsted Acid: Investigation and Application to Synthesis and Catalysis. *J. Am. Chem. Soc.* **2013**, *135* (43), 16213−16219.

(20) Croteau, R. Biosynthesis and Catabolism of Monoterpenoids. *Chem. Rev.* **1987**, *87* (5), 929−954.

(21) Cane, D. E. Enzymic Formation of Sesquiterpenes. *Chem. Rev.* **1990**, *90* (7), 1089−1103.

(22) Köksal, M.; Hu, H.; Coates, R. M.; Peters, R. J.; Christianson, D. W. Structure and Mechanism of the Diterpene Cyclase Ent-Copalyl Diphosphate Synthase. *Nat. Chem. Biol.* **2011**, *7* (7), 431.

(23) Pluth, M. D.; Bergman, R. G.; Raymond, K. N. Acid Catalysis in Basic Solution: A Supramolecular Host Promotes Orthoformate Hydrolysis. *Science* **2007**, *316* (5821), 85−88.

(24) Pluth, M. D.; Bergman, R. G.; Raymond, K. N. Supramolecular Catalysis of Orthoformate Hydrolysis in Basic Solution: An Enzyme-Like Mechanism. *J. Am. Chem. Soc.* **2008**, *130* (34), 11423−11429.

(25) Brown, C. J.; Bergman, R. G.; Raymond, K. N. Enantioselective Catalysis of the Aza-Cope Rearrangement by a Chiral Supramolecular Assembly. *J. Am. Chem. Soc.* **2009**, *131* (48), 17530−17531.

(26) Wang, Z. J.; Brown, C. J.; Bergman, R. G.; Raymond, K. N.; Toste, F. D. Hydroalkoxylation Catalyzed by a Gold(I) Complex Encapsulated in a Supramolecular Host. *J. Am. Chem. Soc.* **2011**, *133* (19), 7358−7360.

(27) Hastings, C. J.; Pluth, M. D.; Bergman, R. G.; Raymond, K. N. Enzymelike Catalysis of the Nazarov Cyclization by Supramolecular Encapsulation. *J. Am. Chem. Soc.* **2010**, *132* (20), 6938−6940.

(28) Leung, D. H.; Bergman, R. G.; Raymond, K. N. Highly Selective Supramolecular Catalyzed Allylic Alcohol Isomerization. *J. Am. Chem. Soc.* **2007**, *129* (10), 2746−2747.

(29) Levin, M. D.; Kaphan, D. M.; Hong, C. M.; Bergman, R. G.; Raymond, K. N.; Toste, F. D. Scope and Mechanism of Cooperativity at the Intersection of Organometallic and Supramolecular Catalysis. *J. Am. Chem. Soc.* **2016**, *138* (30), 9682−9693.

(30) Kaphan, D. M.; Levin, M. D.; Bergman, R. G.; Raymond, K. N.; Toste, F. D. A Supramolecular Microenvironment Strategy for Transition Metal Catalysis. *Science* **2015**, *350* (6265), 1235−1238.

(31) Norjmaa, G.; Marechal, J.-D.; Ujaque, G. Microsolvation and Encapsulation Effects on Supramolecular Catalysis: C−C Reductive Elimination Inside $[Ga_4L_6]^{12-}$ Metallocage. *J. Am. Chem. Soc.* **2019**, *141* (33), 13114−13123.

(32) Prins, H. On the Condensation of Formaldehyde with Some Unsaturated Compounds. *Proceedings of the Huygens Institute—Royal Netherlands Academy of Arts and Sciences*, 1919; Vol. *22*, pp 1919−1920.

(33) Arundale, E.; Mikeska, L. The Olefin-Aldehyde Condensation. The Prins Reaction. *Chem. Rev.* **1952**, *51* (3), 505−555.

(34) Kaphan, D. M.; Toste, F. D.; Bergman, R. G.; Raymond, K. N. Enabling New Modes of Reactivity via Constrictive Binding in a Supramolecular-Assembly-Catalyzed Aza-Prins Cyclization. *J. Am. Chem. Soc.* **2015**, *137* (29), 9202−9205.

(35) Li, N.; Wang, Q.; Zhuo, S.; Xu, L.-P. Mechanism and Origins of Selectivity in the Supramolecular $[Ga_4L_6]^{12-}$-Catalyzed Aza-Prins Reaction: The Mechanistic Studies. *ACS Catal.* **2023**, *13* (16), 10531−10540.

(36) Drudis-Solé, G.; Ujaque, G.; Maseras, F.; Lledós, A. A Computational Study on the Acceleration of the Prins Reaction by Indium Trichloride. *C. R. Chim.* **2004**, *7* (8−9), 885−893.

(37) Alder, R. W.; Harvey, J. N.; Oakley, M. T. Aromatic 4-Tetrahydropyranyl and 4-Quinuclidinyl Cations. Linking Prins with Cope and Grob. *J. Am. Chem. Soc.* **2002**, *124* (18), 4960−4961.

(38) Ogawa, Y.; Painter, P. P.; Tantillo, D. J.; Wender, P. A. Mechanistic and Computational Studies of Exocyclic Stereocontrol in the Synthesis of Bryostatin-like Cis-2, 6-Disubstituted 4-Alkylidenetetrahydropyrans by Prins Cyclization. *J. Org. Chem.* **2013**, *78* (1), 104−115.
(39) Breugst, M.; Gree, R.; Houk, K. Synergistic Effects between Lewis and Brønsted Acids: Application to the Prins Cyclization. *J. Org. Chem.* **2013**, *78* (19), 9892−9897.
(40) Lenardão, E. J.; Botteselle, G. V.; de Azambuja, F.; Perin, G.; Jacob, R. G. Citronellal as Key Compound in Organic Synthesis. *Tetrahedron* **2007**, *63* (29), 6671.
(41) Hart-Cooper, W. M.; Clary, K. N.; Toste, F. D.; Bergman, R. G.; Raymond, K. N. Selective Monoterpene-like Cyclization Reactions Achieved by Water Exclusion from Reactive Intermediates in a Supramolecular Catalyst. *J. Am. Chem. Soc.* **2012**, *134* (43), 17873−17876.
(42) Hart-Cooper, W. M.; Zhao, C.; Triano, R. M.; Yaghoubi, P.; Ozores, H. L.; Burford, K. N.; Toste, F. D.; Bergman, R. G.; Raymond, K. N. The Effect of Host Structure on the Selectivity and Mechanism of Supramolecular Catalysis of Prins Cyclizations. *Chem. Sci.* **2015**, *6*, 1383−1393.
(43) Hyatt, D. C.; Youn, B.; Zhao, Y.; Santhamma, B.; Coates, R. M.; Croteau, R. B.; Kang, C. Structure of Limonene Synthase, a Simple Model for Terpenoid Cyclase Catalysis. *Proc. Natl. Acad. Sci. U.S.A.* **2007**, *104* (13), 5360−5365.
(44) Rudolf, J. D.; Chang, C.-Y. Terpene Synthases in Disguise: Enzymology, Structure, and Opportunities of Non-Canonical Terpene Synthases. *Nat. Prod. Rep.* **2020**, *37*, 425−463.
(45) Davis, A. V.; Fiedler, D.; Seeber, G.; Zahl, A.; van Eldik, R.; Raymond, K. N. Guest Exchange Dynamics in an M_4L_6 Tetrahedral Host. *J. Am. Chem. Soc.* **2006**, *128* (4), 1324−1333.
(46) Breslow, R. Hydrophobic Effects on Simple Organic Reactions in Water. *Acc. Chem. Res.* **1991**, *24* (6), 159−164.
(47) Leung, D. H.; Bergman, R. G.; Raymond, K. N. Enthalpy-Entropy Compensation Reveals Solvent Reorganization as a Driving Force for Supramolecular Encapsulation in Water. *J. Am. Chem. Soc.* **2008**, *130* (9), 2798−2805.
(48) Biros, S. M.; Bergman, R. G.; Raymond, K. N. The Hydrophobic Effect Drives the Recognition of Hydrocarbons by an Anionic Metal-Ligand Cluster. *J. Am. Chem. Soc.* **2007**, *129* (40), 12094−12095.
(49) Dong, V. M.; Fiedler, D.; Carl, B.; Bergman, R. G.; Raymond, K. N. Molecular Recognition and Stabilization of Iminium Ions in Water. *J. Am. Chem. Soc.* **2006**, *128* (45), 14464−14465.
(50) Fiedler, D.; Bergman, R. G.; Raymond, K. N. Supramolecular Catalysis of a Unimolecular Transformation: Aza-Cope Rearrangement within a Self-Assembled Host. *Angew. Chem., Int. Ed.* **2004**, *43* (48), 6748−6751.
(51) Eisenstein, O.; Ujaque, G.; Lledós, A. What Makes a Good (Computed) Energy Profile? In *New Directions in the Modeling of Organometallic Reactions*; Springer, 2020; pp 1−38.
(52) Harvey, J. N.; Himo, F.; Maseras, F.; Perrin, L. Scope and Challenge of Computational Methods for Studying Mechanism and Reactivity in Homogeneous Catalysis. *ACS Catal.* **2019**, *9* (8), 6803−6813.
(53) Tantillo, D. J. Faster, Catalyst! React! React! Exploiting Computational Chemistry for Catalyst Development and Design. *Acc. Chem. Res.* **2016**, *49* (6), 1079.
(54) Chakraborty, D.; Chattaraj, P. K. Confinement Induced Thermodynamic and Kinetic Facilitation of Some Diels−Alder Reactions Inside a CB [7] Cavitand. *J. Comput. Chem.* **2018**, *39* (3), 151−160.
(55) Pahima, E.; Zhang, Q.; Tiefenbacher, K.; Major, D. T. Discovering Monoterpene Catalysis Inside Nanocapsules with Multiscale Modeling and Experiments. *J. Am. Chem. Soc.* **2019**, *141* (15), 6234−6246.
(56) Daver, H.; Harvey, J. N.; Rebek, J., Jr; Himo, F. Quantum Chemical Modeling of Cycloaddition Reaction in a Self-Assembled Capsule. *J. Am. Chem. Soc.* **2017**, *139* (43), 15494−15503.
(57) Goehry, C.; Besora, M.; Maseras, F. Computational Study on the Mechanism of the Acceleration of 1,3-Dipolar Cycloaddition Inside Cucurbit [6] Uril. *ACS Catal.* **2015**, *5* (4), 2445−2451.
(58) Kim, S. P.; Leach, A. G.; Houk, K. The Origins of Noncovalent Catalysis of Intermolecular Diels-Alder Reactions by Cyclodextrins, Self-Assembling Capsules, Antibodies, and RNAses. *J. Org. Chem.* **2002**, *67* (12), 4250−4260.
(59) Li, W.-L.; Head-Gordon, T. Catalytic Principles from Natural Enzymes and Translational Design Strategies for Synthetic Catalysts. *ACS Cent. Sci.* **2021**, *7* (1), 72−80.
(60) López-Coll, R.; Álvarez-Yebra, R.; Feixas, F.; Lledó, A. Comprehensive Characterization of the Self-Folding Cavitand Dynamics. *Chem.—Eur. J.* **2021**, *27* (39), 10099.
(61) Daver, H.; Rebek, J., Jr; Himo, F. Modeling the Reaction of Carboxylic Acids and Isonitriles in a Self-Assembled Capsule. *Chem.—Eur. J.* **2020**, *26* (47), 10861.
(62) Li, T.-R.; Huck, F.; Piccini, G.; Tiefenbacher, K. Mimicry of the proton wire mechanism of enzymes inside a supramolecular capsule enables β-selective O-glycosylations. *Nat. Chem.* **2022**, *14* (9), 985−994.
(63) Capelli, R.; Piccini, G. Atomistic Insights into Hydrogen-Bonded Supramolecular Capsule Self-Assembly Dynamics. *J. Phys. Chem. C* **2024**, *128* (1), 635−641.
(64) Sciortino, G.; Norjmaa, G.; Maréchal, J.-D.; Ujaque, G. Catalysis by Metal−Organic Cages: A Computational Perspective. In *Supramolecular Catalysis: New Directions and Developments*, Wiley, 2022; pp 271−285.
(65) Piskorz, T. K.; Martí-Centelles, V.; Young, T. A.; Lusby, P. J.; Duarte, F. Computational Modeling of Supramolecular Metallo-Organic Cages−Challenges and Opportunities. *ACS Catal.* **2022**, *12* (10), 5806−5826.
(66) Piskorz, T.; Martí-Centelles, V.; Spicer, R.; Duarte, F.; Lusby, P. Picking the Lock of Coordination Cage Catalysis. *Chem. Sci.* **2023**, *14* (41), 11300−11331.
(67) Frisch, M. J.; Trucks, G. W.; Schlegel, H. B.; Scuseria, G. E.; Robb, M. A.; Cheeseman, J. R.; Scalmani, G.; Barone, V.; Petersson, G. A.; Nakatsuji, H.; et al. *Gaussian 16*, 2016.
(68) Becke, A. D. Density-Functional Thermochemistry. III. The Role of Exact Exchange. *J. Chem. Phys.* **1993**, *98* (7), 5648−5652.
(69) Lee, C.; Yang, W.; Parr, R. G. Development of the Colle-Salvetti Correlation-Energy Formula into a Functional of the Electron Density. *Phys. Rev. B* **1988**, *37* (2), 785−789.
(70) Grimme, S.; Antony, J.; Ehrlich, S.; Krieg, H. A Consistent and Accurate Ab Initio Parametrization of Density Functional Dispersion Correction (DFT-D) for the 94 Elements H-Pu. *J. Chem. Phys.* **2010**, *132* (15), 154104.
(71) Andrae, D.; Haussermann, U.; Dolg, M.; Stoll, H.; Preuss, H. Energy-adjustedab initio pseudopotentials for the second and third row transition elements. *Theor. Chim. Acta* **1990**, *77*, 123.
(72) Höllwarth, A.; Böhme, M.; Dapprich, S.; Ehlers, A.; Gobbi, A.; Jonas, V.; Köhler, K.; Stegmann, R.; Veldkamp, A.; Frenking, G. A Set of d-Polarization Functions for Pseudo-Potential Basis Sets of the Main Group Elements Al Bi and f-Type Polarization Functions for Zn, Cd, Hg. *Chem. Phys. Lett.* **1993**, *208* (3−4), 237.
(73) Rassolov, V. A.; Ratner, M. A.; Pople, J. A.; Redfern, P. C.; Curtiss, L. A. 6-31G* Basis Set for Third-Row Atoms. *J. Comput. Chem.* **2001**, *22* (9), 976−984.
(74) Takano, Y.; Houk, K. N. Benchmarking the Conductor-Like Polarizable Continuum Model (CPCM) for Aqueous Solvation Free Energies of Neutral and Ionic Organic Molecules. *J. Chem. Theory Comput.* **2005**, *1* (1), 70−77.
(75) Bryantsev, V. S.; Diallo, M. S.; Goddard, W. A. III Calculation of Solvation Free Energies of Charged Solutes Using Mixed Cluster/Continuum Models. *J. Phys. Chem. B* **2008**, *112* (32), 9709.
(76) Case, D. A.; Aktulga, H. M.; Belfon, K.; Ben-Shalom, I.; Brozell, S. R.; Cerutti, D. S.; Cheatham, T. E., III; Cruzeiro, V. W. D.; Darden, T. A.; Duke, R. E.; et al. *Amber 2021*; University of California: San Francisco, 2021.

https://doi.org/10.1021/acscatal.4c04696
ACS Catal. 2024, 14, 18722−18733

(77) Essmann, U.; Perera, L.; Berkowitz, M. L.; Darden, T.; Lee, H.; Pedersen, L. G. A Smooth Particle Mesh Ewald Method. *J. Chem. Phys.* **1995**, *103* (19), 8577−8593.
(78) Mark, P.; Nilsson, L. Structure and Dynamics of the TIP3P, SPC, and SPC/E Water Models at 298 K. *J. Phys. Chem. A* **2001**, *105* (43), 9954−9960.
(79) Faller, R.; De Pablo, J. J. Constant Pressure Hybrid Molecular Dynamics−Monte Carlo Simulations. *J. Chem. Phys.* **2002**, *116* (1), 55−59.
(80) Norjmaa, G.; Vidossich, P.; Maréchal, J. D.; Ujaque, G. Modeling Kinetics and Thermodynamics of Guest Encapsulation into the $[M_4L_6]^{12-}$ Supramolecular Organometallic Cage. *J. Chem. Inf. Model.* **2021**, *61* (9), 4370−4381.
(81) Wang, J.; Wolf, R. M.; Caldwell, J. W.; Kollman, P. A.; Case, D. A. Development and Testing of a General Amber Force Field. *J. Comput. Chem.* **2004**, *25* (9), 1157−1174.
(82) Heinzelmann, G.; Henriksen, N. M.; Gilson, M. K. Attach-Pull-Release Calculations of Ligand Binding and Conformational Changes on the First BRD4 Bromodomain. *J. Chem. Theory Comput.* **2017**, *13* (7), 3260−3275.
(83) Yin, J.; Henriksen, N. M.; Slochower, D. R.; Gilson, M. K. The SAMPL5 Host−Guest Challenge: Computing Binding Free Energies and Enthalpies from Explicit Solvent Simulations by the Attach-Pull-Release (APR) Method. *J. Comput.-Aided Mol. Des.* **2017**, *31* (1), 133−145.
(84) Babin, V.; Roland, C.; Sagui, C. Adaptively Biased Molecular Dynamics for Free Energy Calculations. *J. Chem. Phys.* **2008**, *128*, 134101.
(85) Babin, V.; Karpusenka, V.; Moradi, M.; Roland, C.; Sagui, C. Adaptively Biased Molecular Dynamics: An Umbrella Sampling Method with a Time-Dependent Potential. *Int. J. Quantum Chem.* **2009**, *109* (15), 3666−3678.
(86) Moradi, M.; Babin, V.; Roland, C.; Sagui, C. The Adaptively Biased Molecular Dynamics Method Revisited: New Capabilities and an Application. *In J. Phys Conf Ser.* **2015**, *640*, 012020.
(87) Barducci, A.; Bussi, G.; Parrinello, M. Well-Tempered Metadynamics: A Smoothly Converging and Tunable Free-Energy Method. *Phys. Rev. Lett.* **2008**, *100* (2), 020603.
(88) Norjmaa, G.; Himo, F.; Maréchal, J.; Ujaque, G. Catalysis by $[Ga_4L_6]^{12-}$ Metallocage on the Nazarov Cyclization: The Basicity of Complexed Alcohol Is Key. *Chem.—Eur. J.* **2022**, *28* (60), No. e202201792.
(89) Sebastiani, F.; Bender, T. A.; Pezzotti, S.; Li, W.-L.; Schwaab, G.; Bergman, R. G.; Raymond, K. N.; Toste, F. D.; Head-Gordon, T.; Havenith, M. An Isolated Water Droplet in the Aqueous Solution of a Supramolecular Tetrahedral Cage. *Proc. Natl. Acad. Sci. U.S.A.* **2020**, *117* (52), 32954−32961.
(90) Le Guilloux, V.; Schmidtke, P.; Tuffery, P. Fpocket: An Open Source Platform for Ligand Pocket Detection. *BMC Bioinf.* **2009**, *10*, 168.
(91) Guerra, J. V.; Alves, L. F.; Bourissou, D.; Lopes-de Oliveira, P. S.; Szaloki, G. Cavity Characterization in Supramolecular Cages. *J. Chem. Inf. Model.* **2023**, *63* (12), 3772−3785.
(92) Ortuño, M. A.; Lledós, A. How Acid Can Become a Dihydrogen Complex in Water? A DFT Study. *J. Organomet. Chem.* **2021**, *949*, 121957.
(93) Bryantsev, V. S.; Diallo, M. S.; Van Duin, A. C.; Goddard, W. A., III Evaluation of B3LYP, X3LYP, and M06-Class Density Functionals for Predicting the Binding Energies of Neutral, Protonated, and Deprotonated Water Clusters. *J. Chem. Theory Comput.* **2009**, *5* (4), 1016−1026.
(94) Su, J. T.; Xu, X.; Goddard, W. A. Accurate Energies and Structures for Large Water Clusters Using the X3LYP Hybrid Density Functional. *J. Phys. Chem. A* **2004**, *108* (47), 10518−10526.
(95) Frushicheva, M. P.; Mukherjee, S.; Warshel, A. Electrostatic Origin of the Catalytic Effect of a Supramolecular Host Catalyst. *J. Phys. Chem. B* **2012**, *116* (45), 13353−13360.
(96) Nguyen, Q. N. N.; Xia, K. T.; Zhang, Y.; Chen, N.; Morimoto, M.; Pei, X.; Ha, Y.; Guo, J.; Yang, W.; Wang, L.-P.; Bergman, R. G.; Raymond, K. N.; Toste, F. D.; Tantillo, D. J. Source of Rate Acceleration for Carbocation Cyclization in Biomimetic Supramolecular Cages. *J. Am. Chem. Soc.* **2022**, *144* (25), 11413−11424.
(97) Andersen, U. N.; Seeber, G.; Fiedler, D.; Raymond, K. N.; Lin, D.; Harris, D. Characterization of self-assembled supramolecular $[Ga_4L_6]$ host-guest complexes by electrospray ionization mass spectrometry. *J. Am. Soc. Mass Spectrom.* **2006**, *17* (3), 292−296.

https://doi.org/10.1021/acscatal.4c04696
ACS Catal. 2024, 14, 18722−18733